Memory as a Topological Structure on a Surface Network

Siddhartha Sen*
Centre for Research in Adaptive Nanostructures and Nanodevices,
School of Physics, Trinity College Dublin, Ireland
Tomas Ryan†
School of Biochemistry and Immunology
Trinity College Dublin, Ireland
David Muldowney‡
Department of Physics, Trinity College Dublin, Ireland
Maurizio PezzoliEmail:maurizio.pezzoli@epfl.ch
Ecole Polytechnique Federale de Lausanne,
Lausanne, Switzerland

Acknowledgment

Siddhartha Sen would like to thank Mike Coey, Kumar Gupta, Mani Ramaswami and Arnab Das for encouragement, Paul Voorheis and Mike Coey for reading through an earlier version of the manuscript and making helpful editorial suggestions. Maurizio Pezzoli would like to thank Raul Ramos for help with the figures. We would like to thank Tim O'Leary for useful comments. David Muldowney would like to thank Christian Klein and Jörg Frauendiener for their kind assistance and for supplying codes used in their work on Riemann surfaces and also to Mauro Ferreira for his guidance and support. This research did not receive any specific grant from funding agencies in the public, commercial or not-for-profit sector.

* Email: sen1941@gmail.com,corresponding author
† Email: tomas.ryan@tcd.ie
‡ Email: dmuldown@tcd.ie

Abstract

A special charged surface network with surface spin half particles on it, that can be arranged in topologically inequivalent ways, is introduced. It is shown that action potential-like signals can be generated in the network in response to local surface deformations of a particular kind. Signals generated in this way carry details of the deformation that create them as a form of plasticity that influences the pathways they traverse leaving a topologically stable helical array of spins: a potential memory substrate. The structure is a non transient alignment of surface spins in response to the transient magnetic field generated by the moving charges present in the action potential-like voltage signals generated since particles with spin have magnetic properties. The structure has a natural excitation frequency that may play a role in memory retrieval. Signal generation and memory storage are proposed to depend on the existence of a surface spin structure. We show that such a surface network can capture the intricate topological features of any connectome in the brain. In addition biophysical properties of such a network are examined in order to constrain predictions of how it may function.

keywords:surface network, solitons, spin structure,memory substrate, topology

Highlights

Global method for generating one dimensional non-dissipative voltage signal pulses, analytic expressions for them with numerical examples, memory substrate creation, memory lifetimes, surface distortion waves.

Introduction

The importance of topology for exploring global features of the brain is now beginning to be recognized in neuroscience and elsewhere. For example there is growing interest in using topological methods to identify hidden structures present in the vast amount of data available that describe the connectivity architecture of the brain's axon network. This is an important area of current research. Another area of exploration where topological and algebraic geometry methods are being used is to unravel the information contained in brain signals. A few representative references in this growing area of research are: (Bassett,2020; Curto,2017; Reimann,2017; K.Hess, 2018; M.Marcolli,2019).

Recently there has also been growing interest in using unconventional ideas to throw light on the functioning of the brain. The aim is to relate global and local features of the functioning brain. We briefly mention two general examples of this nature in which geometric and topological ideas are used. In the first it is suggested that ideas from gauge theories of physics (Sengupta,2016), may help provide a framework for relating local activity of neurons to their system level behavior. Gauge theory converts a global symmetry of a system described by a Lagrangian (O'Raifeartaigh,1997) to one that is local and in the process introduces specific types of local interactions. The underlying geometric structure of gauge theory is that of a mathematical fiber bundle space (Nash,1983). For the brain, the analogue of the Lagrangian, is assumed to be a metastable free energy with a symmetry. The hope is that introducing gauge

theory ideas in such a framework would help tackle problems previously outside the realm of computational neuroscience, such as finding links between action and perception. The scheme described is aspirational and novel but no concrete free energy expression is proposed nor is there a proposal for its symmetry. The major underlying problem addressed is to try to relate the functioning of the brain to its form.

There is also the suggestion that the brain may be regarded as an infinite genus object (Tozzi,2021) where spontaneous creation of Riemann surface networks happen whenever brain signals are generated. A geometrical picture of such a process is suggested where inhibitory neurons are represented by vortex holes which are then given a topological interpretation. The aim of the approach was to understand the functioning of the brain in terms of a global balance between inhibitory(I) and excitatory (E) neurons. A simple geometrical method is proposed to determining the ratio E/I and is carried out. The major idea of the approach is to suggest that a global balance between inhibitory and excitatory neuron activity underpin the functioning of the brain.

In an entirely different area of research, quantum computing, topological ideas are also gaining importance. For example in one influential approach, a topological genus g Riemann surfaces with surface spins has become an area of intense research activity. In these works the aim is to find a way to store and manipulate quantum information that preserves the quantum nature of the system all the time. Quantum systems with large number of atoms or a large number of spins can be made to be in a certain quantum state but

manipulations of the state, necessary to carry out computing, can spoil the quantum nature of the information being processed. There is a need to produce long term stable quantum states. Recent work on a network of spins on a genus g Riemann surface attempts to address this problem by exploiting the inherent stability of topological properties (Hamma,2008). Thus on a genus g Riemann surface two classes of quantum spin configurations are considered, those that form closed loops and those that are not so aligned. Each class of configuration carries an energy label. It is shown that if the strength of an external magnetic field that interacts only with the non aligned spins crosses a critical value, the stable topologically protected lowest energy configuration of the system consists of coherent quantum spins loops rather than of individual spins or open string configurations. This is an example of a topological phase transition. Methods of creating such configurations and their properties are being studied.

In the spirit of searching for global ways of understanding the functioning of the brain, we suggest a scheme in which the form of a special surface network system, represented by its connectivity architecture, can be used to generate action potential-like excitations, by input surface deformations. The scheme proposed differs significantly from existing methods of signal generation, (Scott,2002; Heimburg,2005; Shrivastava,2020) in two important ways: signals are generated by global means where the topology of the surface network and the presence of surface spin half particles play an essential role in generating action potential-like soliton signals. We show that the signals thus

produced carry the surface deformation information that create them and can then transfer this information to the pathways they traverse leaving a non-transient topologically stable helical magnetic structure: a memory substrate. The structure is produced by the alignment of surface spin half particles created by the transient helical magnetic field produced when charge carrying soliton signals move through the network. The memory trace has a natural excitation frequency which can be determined. This leads to the suggestion that memories, stored in this way, may be retrieved by oscillating electromagnetic signals either external or internally generated that have frequencies that overlap with memory label frequencies by a resonance excitation mechanism.

We explain three important features of the scheme: the reason for choosing a special surface for the network, the reason for choosing special type of input signals and how the surface network produces one dimensional action potential-like voltage pulses that are soliton solutions of a special non-linear differential equation called the non-linear Schroedinger equation.

We now prove that the special surface network we choose exactly captures any hypothetical connectome of the brain. It thus captures a important global feature of a brain. Suppose we are given a hypothetical connectome of a specific brain. If this connectome is covered by a smooth surface then a topological theorem, the theorem on classifying surfaces (Munkres,2014) tells us that no matter how complex and intricate are the unknown connection details of the underlying connectome the surrounding surface is topologically equivalent to an orderly array of donut surfaces. Thus the theorem tells us that (Fig 1,

Fig 2A, Fig 3) all represent a Riemann surface. The unknown details of the connectome are reflected by one unknown number of the surface, namely, the number of donut surfaces required to represent it. We will call this mathematical surface an "ubersurface" as it can viewed as a mathematical surface that covers the brain's assembly of three dimensional individual linked neurons. If we suppose the ubersurface is smooth then it becomes a well studied mathematical surface known as a Riemann surface. We will explain what we mean by a smooth surface shortly. The number of donuts g present in the ubersurface is called the genus of the Riemann surface. Thus a Riemann surface which looks like a collection of thin tube like surfaces joined together in regions to form a compact overall structure exactly capture the topology of a given connectome. It captures a global feature of the brain.

There are, however, many smooth non equivalent mathematical Riemann surfaces with spin structure that can capture the brain's intricate connectivity architecture. However within this broad class, it can be proved (Arbarrello,2001) that there is a special subclass of surfaces can generate the wide variety of brain-like signals we want provided this special class of surfaces are charged and have a spin structure. A spin structure means that on the surface there are spin half particles (electrons) that can be arranged in many topologically inequivalent ways. Let us explain this idea by an example. Consider an arrangement of spins in the form of a chain. We view each spin half electron as a magnet and visualized an array of individual spin units as arrows, that represent the north pole to south pole direction of the magnet, linked together,

with all the arrows aligned, that encircles a tube of the surface. The spins are linked by spin-spin magnetic forces. Such an array cannot be changed to one in which the arrow directions are reversed in a continuous way. The two arrays represent two possible spin structures. A given spin structure is topologically stable and cannot be changed by smooth deformations.

The next step is to introduce input signals. An input signal on a surface will be taken to be a local set of surface deformations that are consistent with the mathematical features of the ubersurface. This is physically reasonable as our system is charged surfaces so that surface deformations will lead to local voltage changes. The response of the surface to these deformations is the signal. Surprisingly these are, as we will show, one dimensional soliton solutions of the non-linear Schroedinger equation. Let us explain how such a precise result follows from the qualitative geometrical picture described.

To do this we need two mathematical results. The first tells us that a geometrical charged Riemann surface with spin structure can also be described by an algebraic function called the Riemann theta function where all its variables are constructed from the coordinate variables of the Riemann surface while the spin structure of the Riemann surface is represented in the Riemann theta function by a set of variables called characteristics that can only take two values, namely $(0, \frac{1}{2})$. The charged nature of the Riemann surface makes the theta function a voltage function. The second is that a Riemann theta function associated with a Riemann surface must satisfy an identity called the Fay

trisecant identity (Mumford,1987). It should be noted that the Fay identity holds only if the system has a spin structure.

We now have the concepts needed to explain how signals, as soliton solutions of the non-linear Schroedinger differential equation, can be generated by input surface deformations. The essential idea is to exploit the link between geometry and algebra provided by the Fay identity. This remarkable connection was used by Mumford (Mumford,1987) to find one dimensional soliton solutions of non-linear differential equations. We will discuss this point in greater detailed later. But first we depart from Mumford and show that his solutions can be interpreted as action potential like brain signals. To establish this result requires several steps.

We start by showing that these solutions can be interpreted as signals from one part of our two dimensional Riemann surface network to another. This will be true if our Riemann surface has a modular structure so that signals can be produced in subunits and is the case for our Riemann surface that represent real hyperelliptic equations(Harnack,1876). We next establish the relevance of our network for the brain. This follows from the mathematical result that our surface exactly captures the topological connectivity properties of any hypothetical brain connectome (Munkres,2014) and hence is related to the brain in a very precise way. Finally we interpret local surface pinch deformations as input signals of the network and show that the response of the system to such input signals are soliton solutions of the nonlinear Schroedinger equation if our Riemann surface represents a real hyperelliptic equation and has a spin

structure. Thus Mumford's technical method of finding one dimensional soliton solutions now becomes a method of generating one dimensional soliton in a network.

The dynamical law underpinning our Riemann surface network which leads to these results can now be stated. It is a dynamical principle of compatibility. This requires that all allowed Riemann surface local pinch deformations input signals and the response to them must be compatible with the mathematical structure of the Riemann surface of the network. From this principle, we can show, a wide class of one dimensional signals in response to local pinch deformation signals of different kinds can be generated.

We have outlined how to generate signals by exploiting the form of the surface network and have also described how memories in the form of deformation parameter details can be stored non-locally in a magnetic structure with a frequency label, forming a memory substrate, and how they may be retrieved by a resonance mechanism.

The next step is to to introduce and define the mathematical concepts we need to establish the ideas described. After that we will be able to properly define our ubersurface and pinch deformations, state the dynamical laws of compatibility, and show how pinch deformations can produce one dimensional voltage pulse solutions of the one dimensional non-linear Schroedinger equation. We start by explaining the mathematical ideas required.

Summary of Mathematical Background Ideas

We have already proved that a ubersurface can be chosen to provide an exact topological representation of a particular brain's connectivity architecture captured by its connectome and have said that such a smooth surface is known as a Riemann surface. Our next step is to properly define a Riemann surface. This is done by describing the surface by appropriate coordinates that captures its topological connectivity properties and then introducing mathematical objects that properly describe the smoothness properties of the surface. A useful starting point is a mathematical result that tells us that all Riemann surfaces can be viewed as geometrical representations of polynomial equations (Teleman,2003) of two complex variables, $P(z, w) = 0$, where,

$$P(z, w) = a_0(z) + ...a_i(z)w^i + ...a_m(z)w^m = 0$$

and the coefficients $a_i(z)$ are polynomial functions of z. The degree n of the polynomial, which means the highest power of $n = l + k$ of terms $z^k w^l$ that is present in $P(z, w)$ fixes the genus g of the surface to be $g = \frac{(n-1)(n-2)}{2} - N_s$, where N_s is the number of singular points of the polynomial equation, that is points where $\frac{\partial P(z,w)}{\partial z} = 0$. Thus a Riemann surface is a geometrical representation of a polynomial equation of two complex variables with its genus fixed by the nature of the polynomial. This representation defines the notion of smoothness of the surface as well, where the smoothness of a surface means that there are mathematical objects on the surface that can be differentiated an arbitrary number of times. We then use a mathematical result (Arberello,2001)

that shows that if our ubersurface represents a special polynomial equation called the real hyperelliptic equation and has a spin structure, then pinch deformations can produce a wide variety of one dimensional brain-like signals.

Thus our reason for picking our ubersurface to be a special charged Riemann surface with spin structure is because it exactly captures the topological connectivity of the brain and, by pinch deformations (to be defined shortly) on it, action potential-like signals could be generated by topological means. We thus have a surface network with the topological connectivity properties of the brain which is able to generate action potential-like voltage pulse signals by exploiting its form.

We now proceed to define the mathematical terms introduced: a genus g Riemann surface, Σ_g, its associated the Riemann theta function and show these objects can be constructed from a real hyperelliptic algebraic equation. We also provide a mathematical representation of the deformations, called pinch deformations, of the Riemann surface that generate brain-like solutions of interest.

A Riemann surface Σ_g of genus g with spin structure can be visualized as a smooth spherical surface with g smooth charged tube-like handles (Fig 1) that has electrons on its surface. Bending, stretching or squeezing the sphere or its handles do not change the nature of the Riemann surface as long as these operations are smooth. Consider now a ubersurface that covers the brain's assembly of individual neurons, as described earlier. This surface will have multiple closed loops surrounding voids (Fig 2). The number of these voids

give the genus of the ubersurface. For reasons stated earlier such a ubersurface that captures the connectivity architecture of the brain can be represented by a Riemann surface of high unknown genus value g that can change.

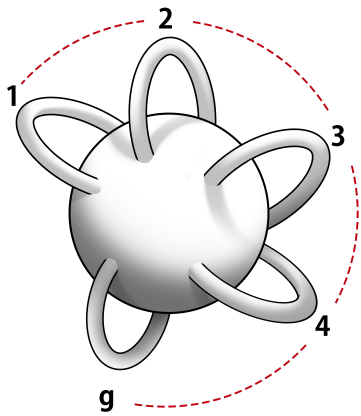

Fig. 1 Genus g surface

Thus the topological connectivity properties of the Riemann surface are displayed in (Fig 2).

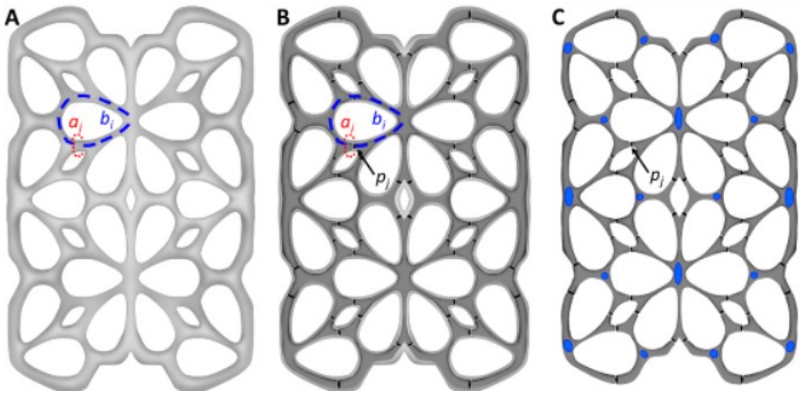

Fig. 2 Riemann surface with coordinate label,Pinched in black, Resultant g=0 surface

Riemann Surface, Σ_g: Representation and Properties

We next explain how the topological connectivity and smoothness properties can be represented. The topological connectivity properties of Σ_g are described by using topological coordinates that are a set of $2g$ closed non-contractible loops $(a_1, a_2, ..a_g : b_1, b_2, ..b_g)$ as displayed in Fig 3. The loops can be selected in different ways, a particular choice of loops is called a marking. The loops chosen have the property that two loops in the set $A = (a_1, a_2, ..a_g)$ or $B = (b_1, b_2, ..b_g)$ do not intersect while a loop a_j from A only intersects with the loop b_j from B. We write these geometric properties as $(a_i, a_j) = (b_i, b_j) = 0, (a_i, b_j) = \delta_{i,j}$, where $\delta_{i,j} = 1$ when $i = j$ and is zero when $i \neq j$ (Fig 3).

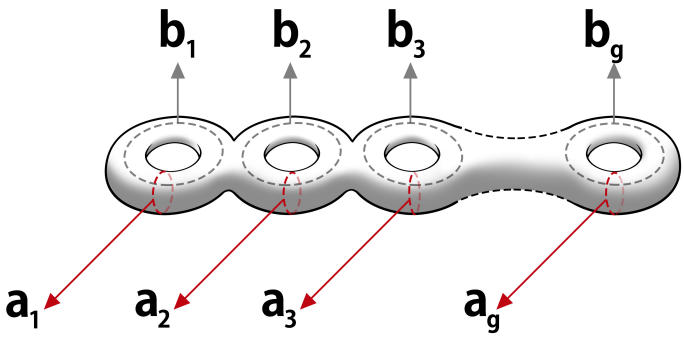

Fig. 3 Marked Riemann surface with topological coordinate loops

The smoothness properties of a Riemann surface Σ_g, with surface points represented by a complex number u, are represented by a set of g linearly independent holomorphic (smooth) differential one forms $\omega_i(u)du, i = 1, 2, ...g$ on Σ_g (Mumford,1987). Since Riemann showed that on a Riemann surface

exactly g linearly independent holomorphic one forms exist, they form a set of basis one forms for Σ_g. This means that any holomorphic on Σ_g can be written as a linear combination of them with constant coefficients. A one form is an object that can be integrated. Thus if we write an integral $\int f(u)du$ then, $f(u)du$ is a one form. Smoothness of the one form means $\omega_i(u)$ can be differentiated an arbitrary number of times with respect to the variable u. In the calculus of complex variables this result follows if $\omega_i(u)$ does not depend on the complex conjugate of u. This result follows directly when a Riemann surface is constructed from a polynomial equation of two complex variables. We will demonstrate how this is done by constructing the Riemann surface that represents a real hyperelliptic equation.

The surface Σ_g, can also be described by an algebraic function called the Riemann theta function. The advantage of this step can be explained by a simple example. Consider the surface of a sphere. It is a geometrical object. If we would like to study how this surface behaves under deformations it is helpful to introduce trigonometric functions. The Riemann theta function plays such a role for studying the dynamical behavior of Σ_g as we will see. Furthermore it easily incorporate the spin structure of Σ_g in terms of a set of $2g$ discrete parameters called characteristics (Mumford,1987). The other variables in the Riemann theta function are constructed from the $2g$ loops and the g smooth (holomorphic) one forms of Σ_g. Thus these variables are constructed using the smoothness and connectivity features of Σ_g. We now define the algebraic Riemann theta function.

The Algebraic Riemann Theta Function

We saw that a Riemann surface Σ_g could be defined in terms of $2g$ loops $(a_i, b_i), i = 1, 2, .g$ and g one forms $\omega_j(u)du$. From these there is a natural way to generate a set of variables (n_i, z_i, Ω_{ij}) as follows. The one forms were normalized so that an integral round a a_i loop $\int_{a_i} \omega_i(u)du = \pm 1_i$. The result represents a winding number associated with the loop a_i. The two signs correspond to the two ways a winding can happen: clockwise or anticlockwise. Thus associated with a loop a_i one can associate a winding n_i, which can take any positive or negative integer values. Next for any given point z of Σ_g it is possible to generate g complex numbers in a natural way by the map $z_i = \int_{z_0}^{z} \omega_i(u)du, i = 1, 2, ..g$ where z_0 is an arbitrary fixed point on Σ_g and we can construct a complex matrix by integrating one forms over b_i loops as $\Omega_{ij} = \int_{b_i} \omega_j(u)du, i, j = 1, 2, ..g$. Riemann proved that this matrix was symmetric and that it's imaginary part was positive. Finally an additional set of variables (α_i, β_i) can be introduced that can only take the values $(0, \frac{1}{2})$. These discrete variables are called characteristics and they represent the spin structure of Σ_g. They allow a fractional windings when going round the a_i, b_i loops which can be shown to be related to the presence of surface particles with spin (Atiyah,1971; Mumford,1971). We can now define the Riemann theta function with characteristics (Mumford,1987):

$$\theta_{[\alpha_i,\beta_i]}(\Omega, z_i) = \sum_{n_1,..n_g=-\infty}^{+\infty} e^{\sum_{a,b} \pi i(n_a+\alpha_a)\Omega_{ab}(n_b+\alpha_b)+2i\pi(z_a+\beta_a)(n_b+\alpha_b)\delta_{a,b}}$$

where $\delta_{a,b}$ is the Kronecker delta function.

The algebraic Riemann theta function is the corner stone of all our discussions. Our one dimensional multi-soliton solutions in Σ_g are expressed in terms of them. In view of this we clarify an important conceptual point. The Riemann theta function depends on g complex numbers $z_i = \int_{z_0}^{z} \omega_i$, generated from two points (z_0, z) on Σ_g. It is thus a g dimensional space of complex numbers, where these numbers have periodicity properties, inherited from the lattice periodicity of the integrals of ω over the closed loops (a_i, b_i) of Σ_g (Mumford,1987). This g dimensional complex space, with the lattice periodicity features factored out, is called the Jacobian, $J(\Sigma_g)$ (Mumford,1987). On the other hand Σ_g is described by just one complex number that represents the points on its surface. Thus the natural question is: how can a theta function represent Σ_g, a function of just one complex variable and how can it produce a one dimensional pulse in Σ_g? There is a helpful mathematical theorem, the Jacobi inversion theorem (Guardia,2002), that answers the first question. It tells us how these two spaces can be related. The basic idea is that for g points on $J(\Sigma_g)$ there are g related points on Σ_g. This theorem is stated in Appendix C.

The answer to the second question comes is that in the pinch deformation limit all of the g complex variables of the theta function collapse to a pair of real numbers that can be interpreted as (x, t), These numbers are multiplied by factors $W_i, V_i, i = 1, 2, ..g$ that represent the nature of the pinch deformation.

Let us give a qualitative account of this result. We start by giving a rough definition of a local pinch deformation at a point z of Σ_g. A more precise

definition of the deformation is given later. Under a pinch deformation the circumference of tube at the pinch point goes to zero and there is a direct link between all g complex variables of $J(\Sigma_g)$ and one complex variable of Σ_g so that the Riemann theta function now directly becomes a function on Σ_g. Let us show how this happens in an intuitive way. Consider a pinch deformation at a point z of Σ_g and examine its effect the g variables z_i of the theta function. These variables are related by the equation $z_i = \int_p^z \omega_i(w)dw$, where z is a point on Σ_g. Now consider a circular arc joining the points z and p of Σ_g. The point p is an fixed point on this circle. In the pinch limit z approaches the p, i.e $z \to p$ as the radius of the circle with center $z = z_0$ inside the tube, shrinks to zero so that the arc length connecting z and p also become small. Thus we have

$$\begin{aligned} z_i &\to \int_p^z \omega_i(w)dw \\ &\to (z-p)\omega_i(z_0) \end{aligned}$$

when z close to p. Since both points, z and p are close to the center of the tube, $z = 0$ we approximated $\omega_i(w)$ by its value at the center of the tube, namely, by $\omega_i(z_0)$. When this is done the g points of the theta function become, $z_i \approx \omega_i(z_0)z$. Thus in the pinch limit all the variables of the theta are all proportional to the point z which is a point on Σ_g close to the center of the tube. We have set $p = 0$. The proportionality factor $\omega_i(z_0)$, defines the nature of the pinch deformation at the point z. Thus a pinch at one point z of Σ

produces g variables of the Riemann theta that are all proportional to a single point z of Σ_g which is close to the centre of the tube.

We next define a hyperelliptic equation and show how it can be used to construct a Σ_g and algebraic Riemann theta function. The hyperelliptic equation has three important features. It allows the maximal possible spin structures on its associated Riemann surface (Krazer,1903). It allows the maximum number of sub unit connected Riemann surfaces allowed (Harnack, 1876). This means it permits a large number of specialized functional subunits of the network to exist, and it can generate a vast number of diverse non-linear excitations by pinch deformations on its subunits [Arberallo,2001; Kalla,2012].

Hyperelliptic Equation, Riemann Surfaces, Theta functions

A real hyperelliptic equation for a genus g Riemann surface is an algebraic equation defined by,

$$\begin{aligned} y^2(u) &= \Pi_{i=1}^{2g+2}(u - x_i) \\ &= P(z) \end{aligned}$$

where u, y are complex numbers but $x_i, 1 = 1, 2, ..(2g + 2)$ are either all real numbers or they occur as a pair of complex conjugate complex numbers. Let us sketch how a hyperelliptic equation describes Σ_g as well as its associated Riemann theta function.

From $P(u)$ to Σ_g

The hyperelliptic equation $y^2 = P(u)$ leads to $y = \pm\sqrt{P(u)}$. Near a zero point x_a of $P(u)$ the function becomes $P(u) = (u - x_a)K$ when all the zeros

are distinct. Setting $w = (u - x_a)$ we have $P(w) = wK$. Thus a circle round $w = 0$ changes the sign of y. It is not well defined. This problem is overcome by introducing a branch cut, a line, that starts at the point $w = 0$ and the rule that when circling round the point $w = 0$ this line cannot be crossed but the variable moves on to another copy of the complex plane. By this means the function y can be made a well defined function of the variable z near all of its zeros. Thus the zeros of $P(u)$ determine (Belokolos,1994) the branch point locations of y that define the cuts necessary to make $y(u)$ well defined. These cuts define the topological coordinates, of the Riemann surface associated with the hyperelliptic equation, namely its homology cycles, $a_i, b_i, i = 1, 2, ..g$ as suitable circuits round the branch points. In particular the a_i cycles, that represent loops round the circumference of tubes of Σ_g, are constructed as circuits round a pair of neighboring zeros of $P(x)$ linked together by a branch cut. We next write down the rule for constructing g smooth one-forms from $P(u)$. We have,

$$\omega_i(u)du = \frac{u^{i-1}du}{\sqrt{P(u)}}, \ i = 1, 2, ...g.$$

Now the complex variable u represents a point on the Riemann surface of genus g constructed. We will replace u by z to represent such points. Thus we have sketched how the topological cycles (a_i, b_i) and the smooth one forms ω_i that define a Riemann surface can be constructed starting from the hyperelliptic equation. It is possible to check that the set of one-forms defined from the hyperelliptic equation are smooth functions, that is they can be differentiated an arbitrary number of times.

From $P(z)$ to the Riemann theta function

We next show how the algebraic Riemann theta function associated with $P(z)$ is constructed. Since we have already sketched how to construct the cycles (a_i, b_i) and the one forms ω_i this is straightforward. We simply have to determine the Riemann theta function variables $(\Omega_{ij}, z_i,)$ and z_i. We have, $\Omega_{ij} = \int_{b_i} \omega_j(z)dz$, and $z_i = \int_0^z \omega_i(w)dw$. The characteristics of the theta function are not fixed by $P(z)$ but are additional structural information about Σ_g that has to be added to the Riemann surface generated by the hyperelliptic equation (Krazer,1901,Kallel,2010).

We are now ready to define our surface network in terms of two postulates and define what is meant by a pinch deformation.

The Surface Network

The network is defined by the following two postulates:

Postulate 1: The surface network is represented by a charged Riemann surface Σ_g with spin structure of genus g associated with a hyperelliptic equation, where g represents the number of Riemann surface loops.

Postulate 2: The surface Σ_g is dynamic and evolving. The response of the surface to local pinch deformations, initiated by mechanical, electrical or chemical means, is determined by requiring them to be compatible with the Riemann surface structure of Σ_g. The responses are the signals of the network. A pinch deformations reduce the circumference of a handle of Σ_g at a point to zero.

We briefly comment on what we mean by compatibility. It simply means that all the mathematical objects introduced are globally defined on the Riemann surface and continue to have this property under deformations.

Pinch deformations

We have already given an informal description of a pinch deformation. Now we give a more precise description of it. Recall a pinch deformation reduces the circumference of a loop handle of the Riemann surface at a point to zero. We define such a pinch on a genus g Riemann surface using its g smooth one forms. There are a number of reasons for this. Firstly, such an approach makes a pinch deformation compatible with the Riemann surface structure of our network since the one forms are all globally defined on the Riemann surface. Secondly, since a one form can be integrated it can naturally be used in an integral along an arc round a central point of a Riemann surface tube that can be shrunk to size zero and hence can be used to describe a pinch. Finally pinch deformations introduced in this way introduce natural deformation parameters.

One forms

We now define a pinch deformation with greater precision. In our applications we will use one forms $\omega_j(z)$ on a Riemann surface that represents a real hyperelliptic equation. We showed that they are given by $\omega_j(u) = \frac{z^{j-1}du}{\sqrt{P(u)}}$ where $P(u) = \Pi_{i=1}^{(2g+2)}(u - x_i)$. Thus these one form depends on the $(2g + 2)$ roots of $P(u)$. We also saw that the a_i cycles of this Riemann surface have circumferences related to the difference between adjacent roots, $(x_{i+1} - x_i)$ of $P(z)$. Hence a pinch corresponds to two roots of the hyperelliptic equation approaching one another as then the circumference of the corresponding loop $a_i \to 0$. The pinch point is taken to be inside the interval. There are g cycles that can be pinched. Thus in applications these details are important. Next

we discuss pinch deformations in a general way. There are g functions $\omega_j(u)du$ whose variables can be deformed differently at a given surface point p. This point has two coordinates $p_a, a = 1, 2$ so that we can write a deformation as $\omega_j(p_a + \delta_{a,j}(p))$. Finally we can write $p = F(z_1, ..z_g) = F(\vec{z})$ as a function of g variables of $J(\Sigma_g)$. This is an inverse of the map $p \to (z_1, ..z_g)$. This function is not known. Putting all these pieces together we can write the pinch deformed one form $\omega_j(p)$, near a pinch point p as,

$$\begin{aligned}
\omega_j(p) &= (V_{a,j}(p) + W_{a,j}(p)k_a(p) + U_{a,j}\frac{k_a(p)^2}{2} + ..)dk_a(p) \\
D_aF(\vec{z}) &= \sum_{j=1}^{g} \partial_{z_j} F(\vec{z}) V_{a,j} \\
\Delta_a F(\vec{z}) &= \sum_{j=1}^{g} \partial_{z_j} F(\vec{z}) W_{a,j}
\end{aligned}$$

The set of points $j = 1, 2, ..g$ represent pinch locations while $k_a(p), a = 1, 2$ can be identified with a point on Σ_g. While the functions $V_{a,j}(p), W_{a,j}(p)$ are the signal specific pinch distortion functions on Σ_g that represent the distortion code of the signal generated. Details of how this procedure is used to prove the Fay trisecant identity and find soliton solutions are given in Kalla (Kalla,2012).

Results

The underlying ideas for generating one dimensional non-dissipative multi-soliton excitations by pinch deformations have already been explained. Let us now write down the solutions, pointing out that they carry pinch deformation information and then show how this information can be transferred and stored non-locally in the form of a topologically stable helical spin-aligned magnetic

trace along paths traversed by the signal. It is substrate structure for memory. The substrate being the pathways traversed by the signal.

Generating Solitons

Pinch distortions have three effects: they increase local voltage values (since the surface is charged), they reduce the original genus g of the system to zero as shown pictorially in Fig 4 and they force the response signal to be one dimensional.

Compatibility Principle and Soliton Signal generation

We would now like to determine the response of the surface to a pinch deformation by using the compatibility principle. The basic idea has already been stated. Namely, that the Riemann theta function describes a Riemann surface only if it satisfies the non-linear Fay trisecant identity given in Appendix A (Arbarello,2001; Raina,1988) and that the Fay identity, deformed by the pinch deformation, becomes a non-linear differential equation. For the deformations we consider, the differential equation is the non-linear Schroedinger equation. Thus the compatibility postulate requires that the Riemann theta function, with its variables distorted by pinch deformations, must satisfy this equation. Thus the response of the surface to a pinch deformation is a theta function solution of the non-linear Schroedinger differential equation.

There are a wide variety brain signal-like soliton solutions that are solutions of the non-linear Schroedinger equation. Thus there are bright soliton trains that are brain spike train-like and dark soliton solutions that are brain burst signal-like. Non-propagating local transient excitations are also possible

solutions of the non-linear Schroedinger equation. The one dimensionality of the solution comes, as we saw, from the fact that a pinch deformation forces surface points to the center of the tube handle pinched. However the solutions do not describe the motion of the pinch point but have a profile determined by the nature of the pinch and the global properties of the Riemann surface that is used to generate it. Here the idea is that a subunit of the Riemann surface generates signals that then propagate to other units connected to it by axons. Such a scheme is possible since a Riemann surface representing a hyperelliptic equation has a modular structure (Harnack,1876).

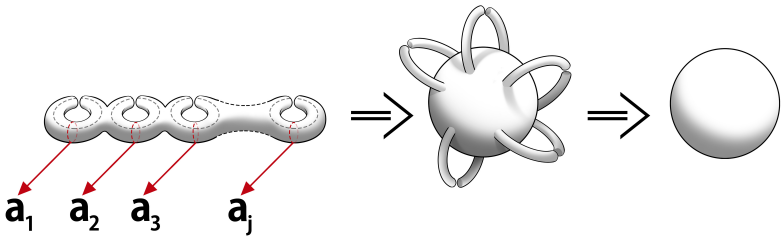

Fig. 4 Degenerate Riemann Surface

Analytic expression for multi-soliton voltage pulses

We now write down multi-soliton pulses solutions (Mumford,1987; Lakshmanan,1995) (Appendix A and B). They can be numerically evaluated (Fig 5). An example of such a solution found by Kalla (Kalla,2012) is:

$$\psi_j(x,t) \;=\; A_j \frac{\theta(\vec{Z}-\vec{d}+\vec{r}(j))}{\theta(\vec{Z}-\vec{d})} e^{-i(E_j x - F_j t)}$$

where $r(j) = \int_{a(n+1)}^{a_j} \omega_j(z)dz$.

$$
\begin{aligned}
\vec{Z} &= i\vec{V}_{a_{n+1}}x + i\vec{W}_{a_{n+1}}t \\
K_1(a,b) &= \frac{1}{2}\frac{\Delta_a\theta[\delta](0)}{D_a\theta[\delta](0)} + D_a \ln\theta[\delta](\int_a^b) \\
K_2(a,b) &= -\Delta_a \ln\theta(\int_a^b) - D - a\ln(\theta(\int_a^b)\theta(0)) - (D_a\ln\theta(\int_a^b) - K_1(a,b))^2 \\
E_j &= K_1(a_{n+1}, a_j) \\
F_j &= K_2(a_{n+1}, a_j) - 2\sum_{k=1}^{n} q_1(a_{n+1}, a_k) \\
q_1(a,b) &= D_a D_b \ln\theta[\delta](\int_a^b) \\
q_2(a,b) &= \frac{D_a\theta[\delta](0)D_b\theta[\delta](0)}{\theta[\delta](\int_a^b)^2}
\end{aligned}
$$

where $\vec{d}, A_j$ are constants. Each pulse solution contains the same pinch deformation parameters through the variable $\vec{Z}$.

It should be noted that n pinches are involved in the solution $\psi_j(x,t)$. Thus a large multi-soliton train is generated by contribution from a large number of pinch deformations. Such a train reflects a global event. We also note that the term $S_j = e^{-i(E_j x - F_j t)}$ where E_j, F_j are constants, present in the solution is a coordinate artifact. This can be seen by multiplying the non-linear Schroedinger equations by S_j^{-1} and defining new variables t', x' by the equations:

$$
\begin{aligned}
\frac{\partial}{\partial t'} &= S_j^{-1}\frac{\partial}{\partial t}S_j \\
\frac{\partial}{\partial x'} &= S_j^{-1}\frac{\partial}{\partial x}S_j
\end{aligned}
$$

Thus $\psi_j(x', t')$ is a solution of the non-linear equation without the factor S_j but now the x', t' variables are j dependent which makes the physical interpretation of a train of solutions is not clear. The soliton trains given by Kalla (Kalla,2012) also do not have the same amplitudes or propagation speeds. These results may be artifacts of Kalla's solutions. We hope to address this issue in future work by directly using biologically relevant boundary conditions to generate solutions. Here we are recording the fact that a wide variety of solutions of the non-linear Schroedinger differential equation exist and that a class of such solutions has been found by Kalla which have brain signal like features that are distorted by oscillatory factors.

Digression on the units and dimensions

An important technical feature of the model is that all the variables, functions and equations used are dimensionless. Thus a direct comparison of theoretical results with observations is not possible. This is also an advantage, because it allows a great deal of flexibility regarding the nature of the system that is being modeled and allows us to interpret the solutions found in terms of voltage pulses as we now show. We have already offered general reasons why the multi-soliton solutions may be interpreted as voltage pulses. Now we use the flexibility of the mathematical equations to show that the solutions can be interpreted as voltage pulses. Consider the following non-linear Schroedinger with dimensional parameters,

$$i\frac{\partial}{\partial t}\psi = -D\nabla^2\psi + g\psi^2\psi$$

where t is in time units, x is in length units, D is a dimensional diffusion constant, ψ is in volts and g is a dimensional constant which is a measure of non-linearity. We can rewrite this equation using dimensionless variables, we have,

$$
\begin{aligned}
t &\to \tau = \frac{t}{t_0} \\
x &\to \frac{x}{x_0} \\
D &\to D_0 = \frac{x_0^2 D}{t_0} \\
g &\to g_0 = \frac{g V_0^2}{t_0}
\end{aligned}
$$

Thus we need to choose three units t_0, x_0, V_0 to compare theoretical predictions with observations. Once chosen, the response solutions generated in the model represent one-dimensional non-dissipative pulses of voltage, and the input signals can also be interpreted as surface deformations that induce voltage changes. Appropriate units of the model can be fixed from observations. Examples of multi-solitons belonging to two different classes, namely light and dark solitons, are numerically determined.

Let us now briefly comment on the way the distortion memory structures appear in our numerical evaluation of multi-soliton solution.

Examples of Multi-soliton solutions

We considered four examples. We note that the oscillatory terms in Kalla's solutions can be eliminated by a coordinate change. In view of this we evaluate ψ_j^2 and numerically checked that it is a soliton for the dark solution and that its inverse is a bright soliton. Two represent bright soliton trains with $g = 2, 3$

and two represent dark solitons that are excitations on top of an elevated background potential (Fig 5). We first found the dark solutions numerically by choosing parameter values and then inverted it and numerically checked that it represented a corresponding bright soliton train solutions. Direct evaluation of these two cases is possible and will be done elsewhere. Here we are simply giving a qualitative feel regarding the nature of soliton solutions. Let us briefly comment on bright and dark solitons.

Solutions of the non-linear Schroedinger equation represent responses, to local pinch deformations of the Riemann surface network. The equation has a non-linear term of the form $\sum_{k=1}^{g} s_k \psi_k(x,t)^2 \psi_j(x,t)$ where $s_k = \pm 1$, for a soltion $\psi_j(x,t)$. Different choices for the sign factor s_k lead to different types of solutions. For dark solutions, of the simplest type, $s_k = +1$ for all k values, while for bright soliton trains $s_k = -1$ for all k values. Other sign selections produce voltage pulse excitations of different shapes and are topologically distinct.

The numerical solution studied fixed the index j of the solutions displayed to $j = 2, j = 3$ to numerically determine two and three dark soliton solutions. The propagation speed of the solitons and their amplitudes found numerically can be adjusted to fit observations by a suitable choice of scale parameters that were discussed. In the case $j = 2$ there are eight and for $j = 3$ twelve distortion parameters. These parameters are assembled together by characteristics, α_i that identify the brain network responsible for the excitation. All characteristics are set to be equal to $\frac{1}{2}$ this means that in the soliton limit all

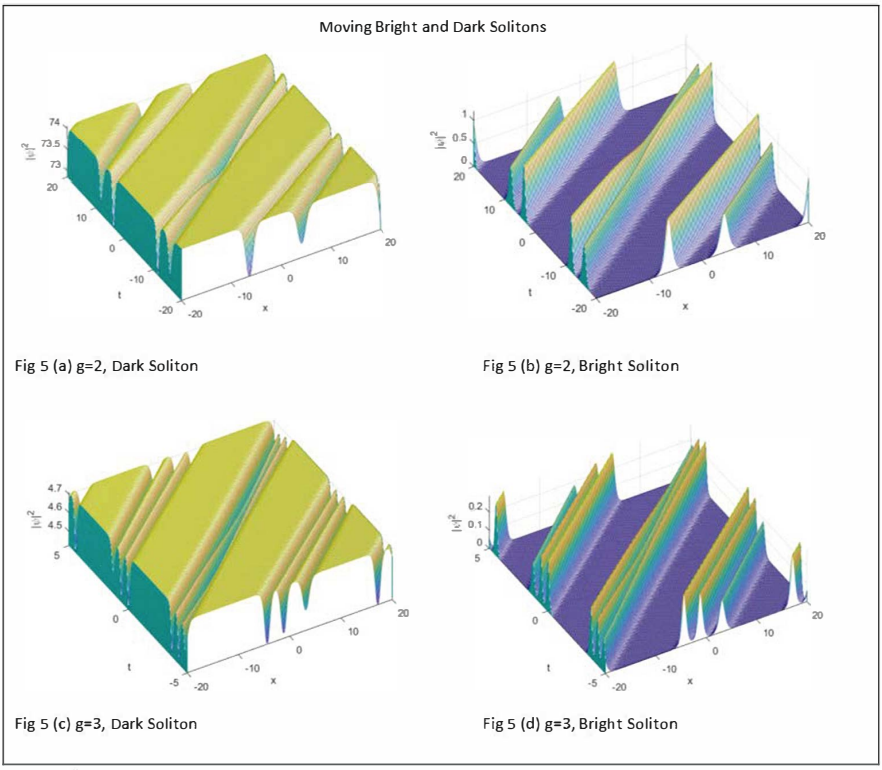

Fig. 5 Moving Dark and Bright Soliton Trains for g = 2, 3.

networks paths of the unit producing the signal are used. We note the vector $\vec{Z}$ fixes the rate at which the spikes arrive. Our numerical results show that gaps between spikes and their rate of production carry memory information as they are sensitive to the pinch distortion parameter values used to generate them. The parameter values for generating the multi-soliton solutions are displayed in Appendix B.

Summarizing: the multi-soliton, excitations have an information carrying substructure that originates from input distortions signal parameters at multiple pinch locations of the surface network. This substructure is carried directly

by the solutions and also indirectly in the appropriate connectivity matrix elements Ω_{ij} of the network responsible for the signal.

We next show how multi-soliton trains can transport and carry the pinch distortion details and how the resultant memory may be stored, at least partially, through non-local topological structures manifest as helical magnetic memory traces along the paths traversed by the multi-soliton.

Helical spin magnetic memory structure formation

We now establish a key result of the surface network, its ability to store the pinch deformation information carried by the soliton pulse signals in static magnetic memory substrates created along pathways traversed by moving, charge carrying, soliton signals. We also show that the structure has a natural excitation frequency that can is determined. This suggests that a memory stored in the memory substrate can be retrieved by any electromagnetic oscillation that has a frequency overlapping with the excitation frequency of the substrate by a process of resonance excitation.That is, memories are labeled by a frequency which can take continuous values. Hence multiple memories can be stored in any pathway. Such a method of storing memory is possible because of two special properties of the surface network: it has a surface spin structure with magnetic properties that can be aligned by the magnetic field produced by soliton signals and because these signals carry with them pinch deformation information of input signals.

The surface network has nothing to say about other methods of storing memories. It suggests a particular approach based on specific assumptions

made that are not as yet firmly rooted in experimental results. A general overview of other approaches is available in Queenan (Queenan,2017). Let us now show that the memory substrate is a static helical alignment of surface spins. Earlier on we showed that it was possible to theoretically determine the voltage profile $\psi(z,t)$ of moving soliton trains along the center line of a tube of the network. We label points of this line by the variable z. By using Poisson's equation (Jackson,1999) of electromagnetic theory, we can directly find the corresponding moving charge profile density $Q_j(z,t)$, that is the charge per unit length, of the soliton pulse voltage profiles. We have,

$$\frac{d^2\psi_j(z,t)}{dx^2} = 2Q_j(z,t)$$

But the charge carried by a soliton pulse is confined to its width as solitons always have a voltage profile as is evident from their explicit form displayed in Appendix B. Thus for a given soliton of pulse of width Δ_j the moving charge is $\frac{dQ_j(z,t)}{dt}\Delta_j$, which we can represent as an effective charge $Q_j(z,0)$ moving with a velocity v_j with $z = v_j t$, where v_j is the speed of the jth soliton pulse moving along the z axis in the center of a tube of the network. Such moving charges create a moving circular transient helical magnetic field as it moves (Jackson,1999), namely a transient helical magnetic field. Thus we have a direct link between the soliton voltage profile and the charge it carries. From this the nature of the magnetic field generated by the jth soliton pulse can be calculated. These helical fields have been calculated and observed (Schoss,2016) but their

effect to align surface spins and the stability of structures produced has not be studied.

We simplify our discussions by replacing the moving charge of a train pulses, $\sum_j \frac{dQ_j(z,t)}{dt}$, by $\sum_j Q_j(z,0)v_j$ and further simplify the expression by replacing it by collection of N moving charges $Q = eN$ with a common velocity v to get a qualitative idea of the nature of the field. Then for a collection of N moving charges along the z-direction inside a tube of radius r_a from the z-axis is, the transient magnetic field is,

$$B_j(z) = \sum_j \frac{Q_j(z = v_j t, 0)v_j}{cr_a^2} \rightarrow \frac{Nev}{cr_a^2}$$

where r_a is the radius of one surface of the cylindrical tube and c is the velocity of light in the medium, using CGS units. If the surface tube has thickness, there are then two cylindrical surfaces both with spin distributions which the magnetic field created by the moving charges can act upon thus creating similar helical structures. We can now write down the explicit form of the two helical surface transient magnetic fields created by the charge moving along the z direction. They are, $h(z, r_{\pm s}) = B_j(z, r_{\pm s}\cos(\frac{2\pi v_j z}{r_{\pm} sc}), r_s \sin(\frac{2\pi v_j z}{r_{\pm} sc}))$, with $z = v_j t, r_{\pm s}$ are the radii of the outer and inner membrane surface of the surface network tube. A multi soliton pulse will generate a transient magnetic field $B(z) = \sum_j B_j(z)$. Since $B(z)$ is determined from the multi soliton profile it contains all the parameters of the multi soliton. These include the pinch deformation parameters that are signal specific as well as the deformed period matrix elements Ω_{ij} that depend on the nature of the Riemann surface.

Surface spins $s_i(z), i = 1, 2$ at the point z of the surface get aligned by the transient magnetic field $B(z,t)$ to form a non transient helical spin structure that captures the helical nature of the transient magnetic surface field created, and hence its profile captures all the parameter details of the multi soliton pulses. It is a memory substrate. It inherits the periodicity of the transient field, with an associated wavelength λ which is determined by requiring $\frac{v\lambda}{cr} = 1$ and also inherits a natural excitation frequency $\omega_1 = \frac{v}{\lambda_n} = \frac{v^2}{cr}$ where v is a allowed soliton pulse velocity. The memory substrate thus formed is topologically stable, since it winds round the surface tube. For a train of soliton pulses with slightly different velocities the memory excitation frequency would be a band of frequencies.

We expect that the memory stored in the substrate can be retrieve by any oscillating electromagnetic signal with a frequency that overlaps with the natural excitation frequency of the substrate. Such an oscillating signal would dynamically excite the natural excitation frequency of the magnetic structure thereby regenerating the stored signal and thus retrieving it. This is a testable prediction of the scheme.

A picture of the helical field of the transient surface magnetic producing a helical spin structure is shown in Fig 6. The helical fields parameters used are all theoretical input values (Table 1). The exact form of the helical curve is not easy to determine. What we show is an idealized sketch using a simple representation of a helical curve, is written as, $B(z,t)(r\cos\omega t, r\sin\omega t, r\omega t)$ which is plotted for two values of r that represent the inner, $R(2)$, and outer

Table 1 Magnetic Helix.

Magnetic Field	Radius(1)	Radius(2)	Frequency
1	2	1.8	1

radii, $R(1)$, of the membrane tube. The magnetic field $B(z,t)$ has a complex shape and is related to the soliton voltage pulse in a way that was determined. The corresponding helical memory substrate is a alignment of spin magnets, as we pointed out.

Finally we observe that creating a magnetic memory trace involves changing the spin structure of the network. This is only possible if the topology of the network is allowed to change as a spin structure is topologically protected. But this is precisely what happens whenever a soliton pulse signal is generated by pinch deformations. Thus the scheme for storing memory in the form of a memory substrate in the connectivity pathways between a set of cells is possible only because signal generations require topological change. A consequence of this picture is the prediction that an external magnetic field would disrupt memory but not modify memory. The external field would act not on individual spin pairs but on the entire spin memory structure leading to local smooth deformations of the structure that do not change its topology.

Biophysical Discussions

We have shown how action potential-like signals that carry a deformation code can be generated from the connectivity architecture of the brain in a two dimensional charged surface network that has a spin structure and have also explained how the deformation code carried by the signals can be transferred

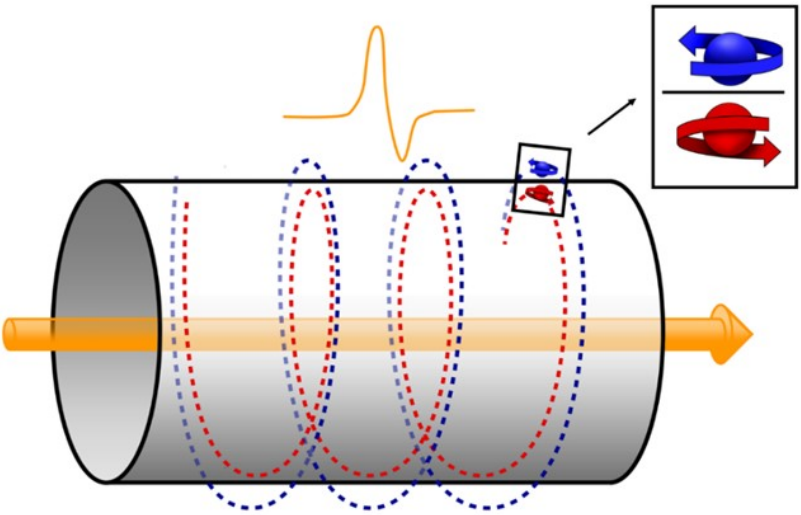

Fig. 6 Helical spin surface structures created by magnetic field of moving solitons where the spins on both surfaces are aligned in the same direction on the surface. The tube shown is part of the surface network.

to the pathways traversed by the signal using the presence of that spin structure and have suggested that memory retrieval might be achieved by a process of resonance excitation where the presence of a frequency label attached to a memory structure is exploited. We now assume that these signals can be identified with brain signals and that the memory storage mechanism suggested is relevant for memory storage in the brain. We would like to explore consequences of such an identification by making a number of numerical estimates. We show that memories stored have a natural excitation frequency, that multi soliton pulses are required to create thermally stable memories and that even though the memory traces are topologically stable they decay.

We start by posing and answering two questions: Is there any biological evidence that supports the assumption that pinch deformations and topology

changes occur when signals are globally generated and can one provide numerical estimates for consequences of the scheme and show that they have realistic biological scales?

The first question is answered by experimental results of Faisal (Faisal,2005) and the other of Ling (Ling, 2020). In the work of Faisal it was shown that brain action potentials were generated if axons were pinched beyond a certain threshold value, while in the electron microscope work of Ling it was found that when a neuron produced an action potential its shape became sphere like. Both these results are consistent with the global pinch method of generating brain signals. The result of Faisal directly confirms that pinch deformations cause action potentials while the result of Ling support the picture that when a signal is generated topological spheres are created. Further evidence of pinching and swelling during action potential generation is found in Costa (Costa,2018).

To tackle the second question we estimate the parameter values and the physical and biological characteristics of our mathematical results using the electrical and geometric properties of the brain axon membrane. In doing this we identify the handles of the Riemann surface as axons, their region of joining with the soma and the pinching points as synapse locations. Since our major hypothesis is that memory is stored as a helical magnetic structure, a memory substrate, on axons created by brain signals traversing through them, we start by making biological estimates regarding the nature of the structure expected on theoretical grounds.

We address the problem in stages. First we estimate the helical memory label frequency and show that it has a value in the range $(2-30+)$ Hz. Then we discuss in greater details binding energy conditions necessary for memory creation, and estimate the lifetimes of memories. In this discussion we will assume that our soliton signals are action potentials. The soliton signals have propagation speeds and amplitudes (voltages) that are theoretically determined, and can be made to agree with the observed values for action potentials simply by choosing suitable scale sizes. Here we show that by using the axon membrane's electrical and geometrical properties we can calculate its resting potential value using the fundamental methods of physics. We also show that as a soliton pulse potential moves inside an axon tube it distorts the axon membrane surface in a way that can be calculated. We derive a formula relating the soliton voltage pulses to membrane distortion wave.

Let us begin with an estimate of the value of the helical frequency ω associated with a memory. We found $\omega = \frac{v^2}{cr}$ where v was the soliton speed, c the velocity of light in the interior of the tube and r the radius of the tube. Substituting a value of $r \approx 10^{-4}$ (Costa,2018) for an axon tube radius, choosing $v \approx 10^3$cm/s (Hursh,1939) as the speed of the soliton and taking c to be in the range $(10^9 - 10^8)$ cm/s, leading to a range of values for ω between $(2 - 30+)$ Hz. The value of c in a medium with ions present can vary over a wide range of values and c can be significantly reduced (Khurgin,2010). This is expected to be the case for light propagating in the ionized fluid environment close to the surface of the membrane tube. The reduction of the value of c is expected

to be considerable since besides having an ionic environment it is known that under pressure the fluid inside a axon tube becomes a gel (Heimburg,2005). There is a phase transition and as a result the speed of light is expected to be decrease significantly. Using these input parameter values we can also estimate the value of $B \approx N_0 \times 10^{-8}$ Gauss, where $N_0 e$ is the charge carried by a single soliton potential pulse.

We next find conditions necessary to create memory and show that the charge transfer by a soliton train has to cross a certain threshold for this to happen. We then show that even topologically stable memories decay due to thermal diffusion and from this estimate memory lifetimes. These are predictions.

Memory Stability

For helical magnetic memory traces to be created the binding energy of spins to the magnetic field generated by the soliton pulse should be strong enough to withstand thermal fluctuations at body temperature T. The binding energy of an aligned pair of spins to the magnetic field generated by a train of N moving charges in the soliton pulse, is given by $U = \mu_B \vec{B}.\vec{\sigma}$, where μ_B is the Bohr magnetron, and $\vec{\sigma}$ the Pauli spin matrices. Using CGS units and physics numbers taken from the National Institute of Standards data base,

$$
\begin{aligned}
U &= \mu_B \vec{B}\vec{\sigma} \\
U &\approx N\,(\frac{10^{-19}}{10^{10}} \times \frac{10^{-6} \times 10^{3}}{(10^{-5})^2}) \\
&= N \times 10^{-28}
\end{aligned}
$$

where N is the number of moving charges in the soliton pulse. This number is tentative as we have used a value for $c \approx 10^9$ cm/s in the medium. We have taken $r \approx \times 10^{-4}$ (Hursh,1939). If we take $N > 10^{14}$ for a muti-soliton pulse, we get a value for the binding energy $U \approx 10^{-14}$ ergs which is of the same magnitude as thermal fluctuation energy. The value of N for multi-solitons is a crude estimate. The actual number is expected to be considerably greater than the bound. The estimate starts from a value for the number of ions that move across 1 μm^2. This is known to be ≈ 6250 (Tansey,2019). Thus the area swept out in one millisecond by the brain voltage pulse is a segment of area $2\pi \times 10^{-4} \times 2$ (taking a action potential to travel with $v \approx 10^3$ m/s and duration 10^{-3} sec). This area contains $N \approx 12 \times 10^7$ charges (Segal,1968). There are $\frac{2\pi 10^{-4}}{2\times 10^{-6}} \approx 10^2$ locations for circles of radius 10^{-6} cm to cover the tubular membrane circumference $2\pi \times 10^{-4}$ cm. Thus the number of charges N per location is 12×10^5 for a single pulse. A multi-soliton must contain over 10^8 pulses for stable memory creation. These numbers can be lowered to $N \approx 10^4$ if the value of c is lowered by environmental effects or if the radius used to locate surface spins has a smaller value.

Our crude estimate suggests that the binding energy of aligned spins per electron is at best only marginally stable under thermal fluctuations. However once formed their topological long range order could make the structure stable. Indeed the spin binding energy, for a helical structure with N spins is, $B_s = N\frac{\mu_B^2}{r^3} \approx N \times 10^{-19} > kT \approx 10^{-14}$ for $N > 10^6$, a condition that can be easily satisfied. The key feature is the topological nature of the aligned spin system

that makes it behave as a coherent unit. We speculate that this is the case for the memory trace and suggest that such a structure might play a role in storing short term or even long term memory in a surface network.

It should also be noted that the estimate given implies that not all soliton pulses will produce stable spin magnetic structures as not all them carry the charge required to produce magnetic fields of the required strength. The magnetic storage of memory in pathways implies that they should be affected by magnetic fields and that these memories can be retrieved by a resonance mechanism using oscillating magnetic fields of low frequency.

Estimate of the Lifetime of Memories

We next estimate the lifetime of memory structures created in the surface network model. The inevitable decay of memories is due to thermal diffusion. The idea is that thermal diffusion inevitably lead to the movement of the particles that carry spin. This movement increases the distance between elements of the magnetic memory trace and eventually lead to their degradation. The random thermal fluctuations lead to the Brownian movement of particles and is represented by the Einstein relation (Einstein,1905):

$$\begin{aligned}(\Delta x)^2 &= 2Dt \\ &= \mu k_B T\end{aligned}$$

where t is time, k_B is the Boltzmann constant, D the diffusion coefficient,μ the mobility coefficient and T the brain temperature. The collection of helically organized spins forms a topological configuration and hence its response to

external disturbances reflects this collective property. For non-durable memory the fluctuating energy due to positional changes of the spins must be greater than the magnetic binding B_M that they have. Now B_M has a length dependence of $\frac{1}{l^2}$ which will also be increased by the fluctuation, that is, $l^2 \to l + \Delta^2 \to l^2 + \mu k_B T$. Putting these pieces together we get,

$$\begin{aligned}
\frac{1}{2}k_s(\Delta x)^2 &> B_M \\
t(k_s k_B T) &> B_M = C_M \frac{1}{(l^2 + (\Delta x)^2)} \\
B_M &= C_M \frac{1}{(l^2 + T\mu k_B)} \\
t &\approx \tfrac{1}{T^2}
\end{aligned}$$

Thus this estimate suggests that lifetime of the non-durable memory depends sensitively on temperature. It should be noted that this Brownian diffusion, with appropriate values for D and μ, is valid for long-term and short term memory and suggests that the Brownian diffusion process will inevitably degrade memory, unless they are periodically consolidated. If we require working memory to have $t \approx 10$ sec and long term memory $t \approx 10^6$ sec (one month), it suggests B_L for long term memory should be $B_L \approx 10^5 B_M$.

Using these ideas an estimate for the number of pulses required to establish a long term memory can be made. Assuming each voltage potential pulse has duration $\approx 10^{-3}$ sec (Hursh,1939) and that the value of B_L is related to total charge transferred by pulses for a month long term memory to be created would require a pulse stream duration of $\approx 10^2$ sec.

We next estimate the electrical properties of the surface network.

Comments on Electrical Features of Surface Network.

We now show, that if we assume that our surface tubes have the known electrical and geometrical properties of the axon membrane we can theoretically estimate the value for the tube's voltage potential. This voltage value will thus estimate the expected resting potential of the system. The calculation uses dynamical laws from quantum electrodynamics. We then show that by introducing additional biological information regarding the presence of fluids inside the surface tubes, a formula linking the voltage pulse propagation in a tube to a surface distortion wave can be found. We start by estimating the equilibrium potential value in a surface tube of the network.

Estimate of Surface Resting Potential Value.

The usual way to estimate the Potential Resting value in biology is by using the generalized Nernst equation based on equilibrium thermodynamics (Sterratt,2014). There the specific equilibrium distribution of sodium and potassium ions was required to model a membrane. Here our aim is different. We want to estimate the equilibrium value between strips of the surface separated by the diameter r of the our surface tube. It is an estimate which only uses the electrical properties and the dynamic laws of quantum electrodynamics (QED) of the tube surface. It was shown by Feinberg (Feinberg, 1970) using QED, that there is an attractive Casimir-Poldar potential $V_{CP}(r)$, between charged dynamic dipoles layers separated by a distance r. The attractive potential is balanced by the elastic properties of the tube and the fluid inside it. We use the observed value r for an axon tube for our surface tube in order to get our

result. We have (Feinberg,1970),

$$V_{CP}(r) = -\frac{V_0}{r^7}$$

which is an attractive potential energy between dynamic neutral molecules. It is the resting potential. Our problem is to estimate the value of V_0, fix the value of r to be the tube diameter r to find the value of V_{CP}. We estimate a value of ≈ 70 mV. Dimensional reasoning is used to estimate V_0.

We use the following notation. Let d be the membrane thickness (Regan,2019), r the diameter of the tube, e the charge of an electron, r_b the hydrogen atom Bohr radius, and N the effective number of molecules in the segment of the membrane chosen. These variables, other than N, are taken to have the following values (National Institute of Standards data base):

$$\begin{aligned} \frac{e^2}{r_b} &= 10 \text{ eV} \\ r_b &= 10^{-7} \text{ cm} \\ r &= 10^{-4} \text{ cm} \\ d &= 10^{-6} \end{aligned}$$

We next write V_0 as

$$\frac{V_0}{r^7} = N^2 \frac{e^2}{r_b} \frac{r_b}{r} \frac{d^6}{r^6}$$

N is determined by setting $V_{CP}(r) = eV_R$, where V_R is the resting potential. Introducing the Bohr radius for hydrogen atom allowed us to set an energy

scale $\frac{e^2}{r_b} \approx 10$ eV. Thus we have

$$\begin{aligned} V_{CP}(r) &= N^2 \times 10 \times 10^{-12} \times \frac{10^{-7}}{10^{-4}} \times (\frac{10^{-6}}{10^{-4}})^6 \text{ ergs} \\ &= 100 \times 10^{-3} \times 10^{-12} \text{ ergs} \\ N^2 &= 10^{13} \end{aligned}$$

Thus we get $N \approx 3 \times 10^6$, which gives an estimate of the number of dipoles in a segment area of the surface. Taking each molecule to have diameter 3×10^{-8} cm the segment length is $\approx 10^{-1}$ cm. Thus the number is roughly the number of lipid dipole molecules per unit area in units of microns (Tansey,2019).

Next we show that by using the Casimir Poldar potential and adding in the biological fact that there is a complex fluid inside the surface network, it follows that multi-soliton voltage pulses $A(x,t)$ must be accompanied by surface distortion waves $\Delta(x,t)$ and a formula relating the two is established.

A Formula for the Surface Distortion Wave

The formula follows from two inputs: a mathematical link between geometric distortions of our surface tube and voltage changes and the appropriateness of using low Reynold number physics for describing the transverse motions of the tube. The first input has already been established by the Casimir Poldar potential. The second input can be easily justified. The Reynold number R of a fluid is given by $R = \frac{\rho v d}{\eta}$, where v is the transverse fluid velocity, d is the diameter of the tube, ρ the fluid density and η the dynamic viscosity coefficient of the fluid. In the transverse direction $d \approx 10^{-4}$cm and v is small so that R is small. In a low Reynolds number environment there are no time delays

and with no inertial effects (Purcell,1977) so that a voltage change directly translates to a deformations in the transverse direction to the propagating voltage pulse (Fig 7).

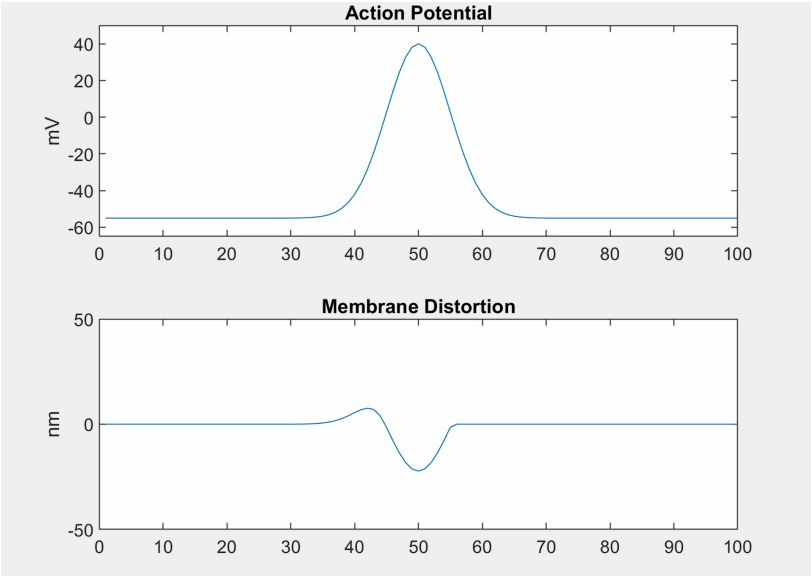

Fig. 7 Predicted Distortion Wave for Rat's Hippocampus Axon radius

Thus the membrane distortion, $r \to r_E + \Delta(x,t)$ where r_E is the equilibrium axon diameter, is proportional to the soliton pulse potential, and we have,

$$\Delta(x,t) = \Delta_T \frac{A(x,t)}{V_T}$$

The proportionality factor is taken to be $\Delta_T \approx r_E \frac{V_E - V_T}{7V_E}$, where V_E is the resting potential, the membrane distortion when $A(x,t) = V_T$, where V_T is the value of the threshold potential, required for a soliton pulse $A(x,t)$ generation. We can only follow the evolution of $\Delta(x,t)$ when it is small compared to r_E.

This condition holds for the cycle of values for $A(x,t)$ that starts and ends at $A(x,t) = V_T$.

If we use our theoretical formula to a biological system we see that the predictions made do give the right range for the distortion wave amplitudes and their speeds. We use $r_E \approx 10^{-4}$ cm, $V_T \approx -65, V_E \approx -80$ mV and the range $-80 < A(x,t) < +20$ mV for the rat's hippocampus axon radius (El Hady,2019) and action potential, our formula predicts that the distortion wave will have $\Delta_T \approx 36, \Delta_M \approx -12$nm. The associated distortion wave is plotted in Fig 7. In the plot we have identified our soliton pulse voltage with the observed action potential pulse voltage recorded. The picture of the distortion wave plotted (Fig 7), uses the parameter values given in El Hady (Table 2). The threshold potential value of -65 mV is an estimate.

Table 2 Distortion Wave Parameters.

Resting Voltage	**Threshold Voltage**	**Reference**
-80	-65	26

A number of different approaches for studying membrane distortion waves have been proposed including electrostriction (El Hady,2019) converse flexoelectricity (Chen, 2019; Petrov,2002) or solitary waves (Anderson,2009; Mussel,2019).

Conclusions

In this paper three significant results have been obtained. The first was proving (Munkres,2014) that there exist smooth surface networks, a Riemann surfaces,

that can exactly capture the topological connectivity properties of any hypothetical brain connectome. Riemann surfaces represent polynomial equations in two complex variables (Teleman,2003) geometrically as surfaces. A Riemann surface is a smooth surface because the polynomial equation that defines it can be differentiated an arbitrary number of times.

The second was to show that for a special subclass of charged Riemann surfaces, related to real hyperelliptic equations, under local pinch surface deformation input signals produce a wide range of one dimensional action potential-like voltage pulse signals provided the charged Riemann surface also had a spin structure. These excitations were soliton solutions of the one dimensional non-linear Schroedinger differential equation. The non-linear Schroedinger equation emerged naturally. It was not an ad hoc add on. The mathematical scheme described produces non dissipative signals and is thus very different from dissipative models of signal generation such as the Hodgkin-Huxley model (Scott,2002).

We called the Riemann surface network an ubersurface as it could be viewed as a mathematical surface covering the brain's assembly of individual three dimensional neurons. Thus a global scheme for generating action potential-like signals using a surface network with the brain's connectivity was shown to be possible. Signals generation exploited the topology and spin structure of the system. To establish this result we had to show that Mumford's (Mumford,1987) soliton solutions on the real line to soliton solutions could be viewed

as signals between the subunits of a given Riemann surface. This was possible since our Riemann surfaces is associated with hyperelliptic equation which is known to have a Riemann surface representation with a modular structure (Harnack,1876). To relate these solitons to brain action potentials we showed that it was possible to make the solitons have observed action potential speeds and peak potential values and by introducing membrane details a dynamical calculation based on quantum electrodynamics was able to provide a good estimate of the axon resting potential value. It was also shown that by using low Reynolds number physics an alternative account for the observed membrane distortion waves observed could be given. These results suggest that the mathematical surface network provides a usedful description of certain brain functions.

It is well known that one dimensional soliton and multi-soliton solutions can be obtained in the real line by a variety of ways Newell(Newell, 1985) but finding them for a one dimensional network faces a number of conceptual problems. For instance the branching details of the network (Yusupov,2019)need to be specified and the boundary conditions for solitons at these junction points need to be fixed resulting in a lack of general network independent results for such systems. In these approaches the choice of the nonlinear system is usually imposed on the network. It is not a natural required feature of the network, unlike the topological surface network where the nonlinear Schroedinger equation emerges from a compatibility principle. This is a surprising and result

that is only valid for a Riemann surface network. Natural soliton signals appropriate for axon tubes exist have been found and investigated (Heimburg,2005; (Shrivastava,2014). The motivation was to see if it was possible to have non dissipative ways of transmitting brain signals. In these approaches the signals were sound like elastic wave solitons that were natural for an axon membrane as they were generated by pinch deformations using the special thermodynamic and elastic properties of fluid of the axon biomembrane. Later it was shown that such signals also induce voltage pulse action potential like signals (Mussel,2019). But these soliton signals do not carry information about the pinch deformations that create them, the nature of pinch deformations required to generate solitons is not clear and extending these solutions to a network or finding producing multi-solitons is problematic. The speed of the solitons are not theoretically determined.

The global approach described here, on the other, utilizes a different global property of the brain. Instead of using the elastic and thermodynamic properties of axon membranes the global approach uses the exact topological connectivity architecture of the brain, captured by a Riemann surface, adds on surface electromagnetic properties and shows how such a system can generate signals in response to surface pinch deformation input signals. Signal generation is now linked to the topology of the system.

The third significant result obtained was to show that the globally produced multi-soliton solutions carry with them the pinch deformation information responsible for their creation as well as information about the network that

created them. The details of the information carried by signals is discussed in Appendix B. The soliton solutions are not point like but have a profile that depends on both the pinch deformation details as well as on the global properties of the ubersurface subunit that created them. They also carry a global topological number $W = \sum_{i=1}^{k} \alpha_i \beta_i$ where $(\alpha_i, \beta_i, i = 1, 2, ..k$ are the characteristics of the theta function related to the global properties of the subunit of genus k pinched to produce a signal. The topological number W reflects the pathways involved in the creation of the signal.

We note that each soliton pulse, of a multi-soliton train, carries the same pinch deformation information and we showed how these pulses can transfer this information to the pathways they traversed in the form of strands of a topologically stable helical spin aligned magnetic trace that have a natural, theoretically estimated, excitation frequency.

We also showed that a single pulse cannot produce a stable memory trace. Since the memory strands carry a continuous frequency label multiple memories can be stored in a given pathway. Thus the scheme suggests that memory retrieval could operate by a resonance excitation mechanism that exploits the presence of memory excitation frequency bands. This prediction is testable. The idea of storing memory in a magnetic structure in the scheme is a strong assumption. It requires the presence of sufficient number of surface electrons in the brain to be viable. There are free electrons in the brain but their numbers and distributions are not known. Whether memory storage is in spin structures or not will ultimately have to be resolved by experiments.Such helical

arrays of spin have been found in condensed matter physics (Uchida,2006). In our approach the soliton signals carry information directly. In a widely used approaches (Bialek,1991) it is suggest that information in a train of acction potentials is hidden in the frequency of action potential production and/or in the distribution of a train of action potentials.

Let us briefly comment on the existing mechanism suggested for storing memory. One review (Queenan,2017) discusses the difficulty of understanding long term memory storage in the brain by examining different mechanistic hypothesis that have been proposed, with various degrees of supportive evidence. The most widely accepted suggestion is that memory is stored by changing the magnitude of synaptic weights (Kandel,2019; Ortegao de San Luis, 2022). However, recent studies indicate that this form of plasticity may be important for memory encoding and retrieval, but is dispensable for long term information storage itself (Tonegawa,2015). Another hypothesis posits that memory is stored in an intracellular level by chemical means (Glanzman,2018; Gershmann,2021). However this view faces an immediate problem, as most mammalian proteins exist for a few days while synaptic proteins likely to be relevant, can manage to live maybe up to a week (Tsien,2013). There are few plausible candidate proteins currently available that can play such a role, and there is no clear mechanism for quickly storing information in such long lived objects such as polynucleotide chains (but see Akhlaghpour, 2022). A viable system exists that plasticity of synaptic wiring between cells may alter the connectome to store a stable memory as stable microanatomical engrams

(Ryan, 2021). Though plausible this hypothesis provides only a substrate for engram formation but no clear insight into information coding. In view of this impasse, alternative unconventional but testable suggestions such as the one suggested in this paper may be appropriate.

The mathematical scheme also has geometrical implications. A direct correspondence between the parameters of the hyperelliptic equation and the location of synapses and dendrites and the roots of the hyperelliptic equation can be made. Synapses and dendrites are located near junction points of the surface that represent the soma, they themselves correspond to pairs of points on the b_i cycles of the ubersurface that are determined by the zeros of the hyperelliptic equation while a pair of adjacent zeros of the equation define the a_i, the circumference of a loop round an axon tube. These features follow from the way we constructed the (a_i, b_i) loops from the hyperelliptic equation.

Summarizing one can say that all the results of the surface network come from its topology, smoothness and its spin structure and that in the scheme there is a direct mathematical link between the trinity: signals-information-memory. The spin structure is, as explained, essential for signal generation and for providing a memory substrate in the pathways connecting special memory cells. We also stressed that signal generation in the scheme requires that the genus g of a subunit producing the signal must change to genus zero: thus producing transient spherical surface that are in excited electrical states. This is a prediction of the scheme that should have observable consequences which we plan to investigate.

Declarations

1. This research did not receive any specific grant from funding agencies in the public, commercial or not-for-profit sector.
2. The authors declare no competing financial interests.
3. Availability of data and methods (not applicable)
4. Code supplied by C.Klein and J.Frauendiener.
5. Contribution of Authors: Siddhartha Sen developed the model and wrote the paper, David Muldowney carried out the numerical calculations, to produce the soliton and distortion wave figures, Tomas Ryan and Maurizio Pezzoli contributed to the writing and suggested key neuroscience ideas. Maurizio Pezzolli produced all the remaining figures and Tomas Ryan edited the text.

Supplementary Material

Appendix A: The Degenerate Fay Trisecant Identity

The soliton solutions were found by exploiting a link between the Riemann surface and the Riemann theta function provided by the Fay identity. In the logic chart these links are shown. In it the Fay trisecant identity is also displayed using the notation of (Raina,1998). Here we write down the pinch degenerate limit of the Fay identity due to (Kalla,2012):

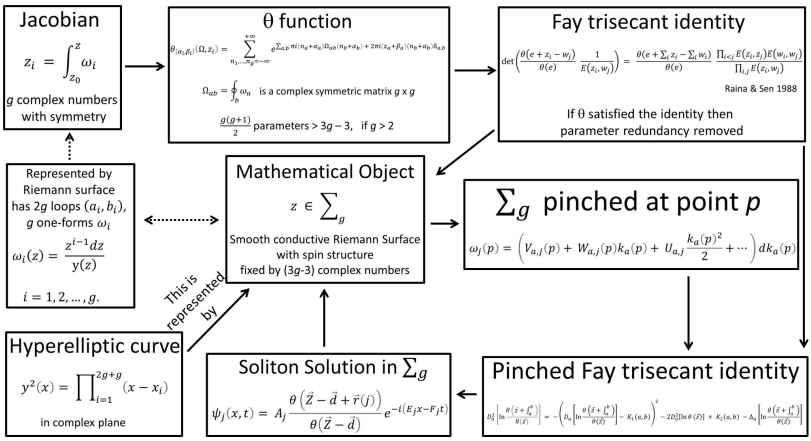

Fig. 8 Chart of Logical links.

We define the functions we need to write down the degenerate form of the Fay identity. Let a, b be distinct points on Σ_g. Fix local parameters k_a, k_b in a neighborhood of these points. Let $\delta = (\alpha_i, \beta_i), i = 1, 2, ..g$ be a non-singular odd characteristic. Then for any $\vec{z} = (z_1, ..z_g)$, Fay's identity is $A = C + D + E$ where

$$\begin{aligned} A &= D_a^2[\ln \frac{\theta(\vec{z} + \int_a^b)}{\theta(\vec{z})}] \\ C &= -(D_a[\ln \frac{\theta(\vec{z} + \int_a^b)}{\theta(\vec{z})}] - K_1(a,b))^2 \\ D &= -2D_a^2[\ln \theta(\vec{z})] + K_2(a,b) \\ E &= -\Delta_a[\ln \frac{\theta(\vec{z} + \int_a^b)}{\theta(\vec{z})}] \end{aligned}$$

where $\int_a^b = \int_a^b \vec{\omega}$ and the scalars $K_1(a,b), K_2(a,b)$ are given by

$$\begin{aligned} K_1(a,b) &= \frac{\Delta_a \theta[\delta](0)}{2D_a \theta[\delta](0)} + D_a \ln \theta[\delta](\int_a^b) \\ K_2(a,b) &= -\Delta_a \ln \theta(\int_a^b) - D_a^2 \ln(\theta(\int_a^b)\theta(0)) - (D_a \ln \theta(\int_a^b) - K_1(a,b))^2 \end{aligned}$$

where D_a is the operator of directional derivate along the vector $\vec{V} = (V_{a,1}, V_{a,2}..., V_{a,g})$ while Δ_a is the operator of directional derivative along the vector $\vec{W} = (W_{a,1}, W_{a,2}..., W_{a,g})$ where these vectors describe the pinch distortion at a point of Σ_g. Thus Fays identity is written down for a specific pinch deformation.

Next we recall that the parameters of the pinch deformation at a point p of Σ_g are given by the vectors $(\vec{V}, \vec{W})$, as follows,

$$\omega_j(p) = (V_{a,j} + W_{a,j} k_a(p) + U_{a,j} \frac{k_a(p)^2}{2} + ..) dk_a(p)$$

$$D_a F(\vec{z}) = \sum_{j=1}^{g} \partial_{z_j} F(\vec{z}) V_{a,j}$$
$$\Delta_a F(\vec{z}) = \sum_{j=1}^{g} \partial_{z_j} F(\vec{z}) W_{a,j}$$

where the set of points $a_j, j = 1, 2, ..(g+1)$ represent pinch locations. They are special points of Σ_g related to the location of the zeros of the hyperelliptic equation. The representation of the one form $\omega_j(p) = V_{a,j} + W_{a,j} k_a(p) + ...)dk_a(p)$ parametrize the signal specific deformations while the range of the label j captures the number of pinch points that contribute to the soliton excitation. Using this notation multiple component (spike trains) solutions of the non-linear Schroedinger equation, found by Kalla (Kalla,2012) can be written down. We are interested in the soliton limit of this solution.

Appendix B: Soliton Limit

Soliton solutions emerge in the limit when a genus g surface degenerates to one of genus zero. The technical way of doing this is discussed in Kalla (Kalla,2012). As a genus zero surface is conformally equivalent to Riemann sphere there is a map $w(p) = w$ which maps a point p on the genus zero surface to a point w on the Riemann sphere. In the genus zero limit we have the following result,

$$\Omega_{kk} = \ln \epsilon + O(1)$$
$$\Omega_{ik} = \ln[\frac{(w_i - w_k)(s_i - s_k)}{w_i - s_k)(s_i - w_k)}]$$

The diagonal period matrix elements expression from $\Omega_{kk} = \int_{u_i}^{v_i} \Omega_{v_k - u_k} + O(\epsilon)$ where $\Omega_{v_k - u_k} = (\frac{1}{w - w_{v_i}} - \frac{1}{w - w_{u_i}}$ and u_i, v_i are poles that appear when double points that result when the genus g surface degenerates to one of genus zero

are desigularized. The meromorphic differentials that then appear on the topological sphere are entirely defined by their behavior near their singularities. In this pinching limit meromorphic functions also appear associated with the variables z_i regarded as functions of a point z of the Riemann surface. The reason for the appearance of singularities can be easiliy understood. A pinch deformation corresponds to the shrinking of a_i loops of a Riemann surface. These loops correspond to circuits round neighboring zeros of the hyperelliptic equation $y^2 = \Pi_{i=1}^{(2g+2)}(z - x_i)$ that define branch points of the equation in the complex plane. Thus a pinch deformations correspond to two zeros coming $(x_i, x_{i+1}$ together. When this happens the associated one forms $\omega_j(z) = \frac{z^j dz}{\sqrt{P(z)}}$ become singular and so do the function $z_i = \int_0^z \omega_j(z)dz$ since $P(z)$ now becomes $P(z) \to \Pi_{i=1}^{(1=g}(z - w_i)$. One technical point is that the expression for $\omega_i(z)dz$ written down in terms of the hyperelliptic function needs to be normalized before it can be used in the theta function.

The general structure of such a meromorphic function $f(w)$ is, now,

$$f(w) = \alpha \Pi_{i=1}^{(n+1)} \frac{w - w_{a_i}}{w - w_{b_i}}$$

with a local parameter $k(w_a) = f(w) - f(w_a)$, where we also require that $f(w_{u_k}) = f(w_{v_k}$. This requiement comes from a global constraint that the distortion parameters have to satisfy. With the help of these variables we can explictly identify the memory parameters. They are the distortion parameters and the location of poles of one forms and the location of poles and zeros of the meromorphic functions. These parameters thus describe the nature of

distortions and they also carry information about the network by carrying information about the location of pinch points and the deformed period matrix.

For our case $w_a = w_{a_{n+1}}, w_b = w_{a_j}$. We have

$$\begin{aligned} V_{a,k} &= \frac{1}{k_a'(w_a)}[\frac{1}{w_a - w_b} - \frac{1}{w_a - w_{u_k}}] \\ W_{a,k} &= A_{a,k} + B_{a,k} \\ A_{a,k} &= \frac{1}{k_a'(w_a)^2}[-\frac{1}{(w_a - w_{v_k})^2 + \frac{1}{(w_a - w_{u_k}})^2} \\ B_{a,k} &= -\frac{k_a''(w_a)}{k_a'(w_a)^2} V_{a,k} \end{aligned}$$

where $V_{a,k}, W_{a,k}$ are pinch deformation functions. Then the theta function becomes

$$\begin{aligned} e^{[\sum_{i,k=1}^{n+1}(i\pi\Omega)_{ik}\alpha_i\alpha_k + \sum_{k=1}^{n+1} 2i\pi\alpha_k z_k]} &= det(T) \\ (T)_{ik} &= \delta_{ik} + \frac{w_i - s_i}{w_k - s_k} e^{z_i + z_k} \end{aligned}$$

where each characteristic, $\alpha_i, i = 1, 2, ..(n+1)$ can only be either $0, \frac{1}{2}$ and $z_k^j = Z_k - d_k + \beta r_{j,k}, Z_k = iV_{a_{n+1},k}x + iW_{a_{n+1},k}t$ The other variables $r_{j,k} = \ln \frac{[(w_b - w_{v_k})(w_a - w_{u_k})]}{w_b - w_{u_k})(w_a - w_{v_k})]}$ and β is a constant that can take values $(-1, 0 + 1)$ while the parameters d_k are constants.

In terms of these variables the dark soliton train , $\psi_j(x,t), 1 \leq j \leq n$ solution (Kalla,2012) of the non-linear Schroedinger equation can be written as,

$$\psi_j(x,t) = A_j e^{i\theta} \frac{det(T_{j,1})}{det(T_{j,0})} e^{-i(E_j x - F_j t)}$$

where A_j, E_j, F_j are known constants (Kalla,2012). The soliton variables depend on the parameters,$(w_i - s_i)$ and the variables z_i that explicitly depend on the deformation parameters $V_{a,k}, W_{a,k}$, while the set of non zero characteristics carry information about the network responsible for generating the signal. The deformed period matrix also appears in the solutions.

We illustrated the approach by numerically evaluating four multi-solitons. In all the cases we use the fact that the oscillating factor is a coordinate artifact, as we showed and plot the absolute value of the non-oscillating part. We plan to present solutions without oscillation terms in a future work. Here we find first dark solutions for $g = 2, g = 3$ and then invert it to get a bright multi-solitons (Figure 7). The soliton nature of both solutions is shown numerically.

Dark solitons are special high energy excitations that can come from a small cluster of pinches in a background of high excitation. Their shape is thus an elevated potential hump on top of which there are oscillations.

In the numerical evaluations of the two and three spike multi-soliton solution for dark and bright multi-solitons are considered and it is found that not all input signal parameters lead to excitations. This is an intriguing result. The solution's pinch deformation parameters fix the rate at which the soliton spikes appear as well as the gaps between them through the parameters $\vec{Z}$ and $\vec{r_j}$ of the solutions while the parameters $T_{j,\beta}$ fixes the spike shapes. We write $V = (a_j, b_j) = a_j + ib_j, W = (c, d) = c + id, i = +\sqrt{-1}, j$ and $(V_j, W_j) = (a_j, b_j, c_j, d_j), j = 1, 2, 3$ The pinching loops, for the, $g = 3$, dark solitons, are real points $(a_1 = -3.999, a_2 = -3.95, a_3 = -3.92, a_4 = -3.91)$,

Table 3 g=3 Dark Soliton Parameters

Synapse	Code	Network	T or E
Synapse(1)	$(0, -2.5873, 0, 11.5975)$	$(1, 1, 1)$	T
Synapse(2)	$(0, -3.09581, 0, 14.706)$	$(1, 1, 1)$	T
Synapse(3)	$(0, -3.2384, 0, 15.6638)$	$(1, 1, 1)$	T

they are the zeros of the hyperelliptic equation. The Riemann surface is constructed using this information and choosing branch point locations in the complex plane located to be: $(-4, -3, -2, -2+\epsilon, 0, 0+\epsilon, 2, 2+\epsilon), \epsilon = 10^{-10}$. The input data is displayed in tabular form in Table 3. For the $g = 2$ case the branch points are $(-2-1, 0+\epsilon, 2+\epsilon)$, the pinching loops are $(a_1 = -1.9, a_2 = -1.11, a_3 = -1.8)$ and input distortion data is displayed below,

Table 4 g=2 Dark Soliton Parameters

Synapse	Code	Network	T or E
Synapse(1)	$(0, -1.9142, 0, 2.5916)$	$(1, 1)$	T
Synapse(2)	$(0, -2.2790, 0, 3.6734)$	$(1, 1)$	T

Appendix C: The Jacobi Inversion Theorem

The equivalence of Σ_g and $J(\Sigma_g)$ is at the level of certain abelian groups called divisors. For Σ_g a divisor D is the formal sum of selected points on Σ_g mutiplied by integers. These groups establish a relationship between the number of zeros of functions on Σ_g to the corresponding number of zeros of the Riemann theta function on $J(\Sigma_g)$. We have,

$$D = \sum_p n_p p$$

The degree of a divisor is defined as $\deg D = \sum_p n_p$. For a meromorphic function $f : \Sigma_g \to C$ a natural notion of a divisor (f) can be introduced. We

write

$$(f) = \sum_p (\mathrm{ord}_p(f))_p$$

This is an enrichment of Σ_g as further structures namely special types of functions are introduced on it. A meromorphic function has simple zeros and poles. The order at a simple pole is minus one while at simple zero it is plus one. A general result is that the sum of the orders of zero and poles of a meromorphic function on Σ_g is zero. This translates to the statement that $\deg(f) = 0$. We next introduce the Abel-Jacobi map that maps points p on Σ_g to points on $J(\Sigma_g)$. Remember a point in $J(\Sigma_g)$ is defined by g complex numbers. We have,

$$\begin{aligned} \mu : \Sigma_g &\rightarrow J(\Sigma_g) \\ \mu &= (\int_{p_0}^{p} \omega_i, i = 1, 2, ..g) \end{aligned}$$

The point p_0 is a fixed reference point on Σ_g with respect to which other points are linked by a path. It is possible to show that the linking path chosen does not matter. The map is well defined.

This map extends to divisors. For points p in Σ_g we have,

$$\mu(\sum_p n_p p) = \sum_p \mu(p)$$

We can now state the inversion Jacobi theorem.

Jacobi Inversion Theorem

For every point in $J(\Sigma_g)$ is the image under μ of a degree zero divisor of the form $D = \sum_{i=1}^{g}(p_i - p_0)$ on Σ_g

References

[1] Akhlagpour, H., An RNA-based theory of natural universal computation, Journal of Theoretical Biology, Vol 537, 110984 (2022).

[2] Anderson,S., Jackson, A.D, Heimburg, T., Towards a thermodynamic theory of nerve pulse propagation, Progress in Neuroscience, 88, 104-113 (2009).

[3] Arbarello,E. Sketches of KdV, Contemporary Mathematics, 312, 9-70 (2001).

[4] Atiyah, M., Spin Structures, Ann.Scientifique de l'Ecole Normale Superieure, Quatrieme, Series, 4, 47-62 (1971).

[5] Belokolos, Algebraic geometry approach to non-linear integrable equations, Springer series in non-linear dynamics (1994).

[6] Bievins, A.S., Bassett, D., Topology in Biology, ISBN:978-3-319-70658-0 (2020).

[7] Bialek,W.,Rieke,F.,de Ruytes van Steveninck,B.R,,Warland,D., Reading a neural code,Science,252(5014),1854-7,(1991)

[8] Chen, H., Garcia-Gonzalez and Jerusalem, A., A computational model of the mechanoelectrophysiological coupling in axons with applications to neuromodulation, Physical Review E, 99, 032406 (2019)

[9] Costa, A. R., Pinto-Costa, R., Sousa, S. C., and Sousa, M. M., The Regulation of Axon Diameter: From Axonal Circumferential Contractility to Activity-Dependent Axon Swelling, Frontiers in Molecular Neuroscience, 11, 319. https://doi.org/10.3389/fnmol.2018.00319 (2018).

[10] Curto, C., What can topology tell us about the neural code? Bulletin of the AMS, 54, 63-78 (2017).

[11] Einstein, A., Investigation on the theory of Brownian movement, Dover Publications (1905).

[12] Faisal, A., White, J., Laughlin, S., Ion-channel noise places limits on the miniaturization of the brain's wiring, Current. Biol, 15(12), 1143-9 (2005).

[13] Fay, J., Theta functions on Riemann surfaces, Lectures Notes in mathematics, 352 (1973).

[14] Feinberg, G., Sucher, J., General Theory of van der Waals Interaction: A Model Independent Approach, Phys. Rev. A, 2, 295 (1970) .

[15] Guardia, J., Jacobian nullwerte and algebraic equations, Journal of Algebra , 253 112-132 (2002).

[16] Gershman, S., Balbi, P., Gallistel, C., Gunawardena, J., Reconsidering the evidence for learning in single cells, eLife 2021 Jan 4;10:e61907. doi:10.7554/eLife.61907 (2021).

[17] Glanzman, D., Bedecarrat, B., Chen, S., Pearse, K., Cai, D., RNA from Trained Aplysia can Induce an Epigenetic Engram for Long-Term Sensitization in Untrained Aplysia, eNeuro 2018 May-Jun:5(3): ENEURO.0038-18.2018 (2018).

[18] El Hady, A., Machta, B., Mechanical Surface waves accompany action potential propagation, Nature Communications, doi:10.1036/ncomms7697 (2019).

[19] Hamma. A., Lidar, D., Adiabatic Preparation of Topological Order, PRL

100,030502 (2008) .

[20] Harel,A., Ryan, T., The memory toolbox: how genetic manipulations and cellular imaging are transforming our understanding of learned information, Current Opinions in Behavioral Science, 136-147 (2020).

[21] Harnack, A., Uber die Vieltheiligkeit der ebenden algebraischen Curven, Mathematische Annalen, 10, 189-198 (1876).

[22] Heimburg, T., Jackson, A., On Soliton Propagation in biomembranes and nerves, PNAS, doi:10.1073/pnas.0503823102 (2005).

[23] Kanari, L., Dlotka, P., Scolamiero, M., Levi, R., Hess, K., Shillcock, J., Markham, H., A topological representaion of branching neuronal morphologies, Neuroinformatics, 16, 3-13 (2018).

[24] Hodgkin, A., Huxley, A., Action potential recorded from nerve fibre, Nature, 144, 710-11, (1939).

[25] Hursh, J., Conduction velocity and diameter of nerve fibers, Americal Journal of Physiology, 127 (1939).

[26] Jackson, J. D., Classical Electrodynamics, p134, John Wiley and Sons (1963).

[27] Kalla, C., New Degeneration of Fay's Identity and its Applications to Integrable Systems, International Mathematical Research Notices, Vol 2013, Issue 18, DOI:10.1093/imrn/rns175 (2012).

[28] Kallel, S., Sjerve, D., Invariant Spin Structures for Riemann Surfaces, Annals of the Faculty of Sciences of Toulouse:Mathematics, Series 6, Vol 19, 457-477 (2010).

[29] Kandel, E., Ashok, A., Leroy, F., Rayman, J., Molecular Mechanisms of the Memory Trace, Trends in Neuroscience, Vol 42, 14-22 (2019).

[30] Khurgin, J., Slow light in various media, Advanced Optics and Photonics, Vol2, Issue 3, 287-318 (2010).

[31] Krazer, A., Lehbruch der Thetafunktionen, Verlag von B.G., Teuner (1903).

[32] Radhakrishnan, R., Shahadevan, R., Lakshmanan, M., Integrability and Singularity structure of coupled non-linear Schroedinger equations, Chaos, Solitons and Fractals, Vol 5, Issue 12, 2315-2327 (1995).

[33] Ling, T., Boyle, K., Ramakrishnan, C., Deisseroth, K., High Speed interferonectric imaging reveals dynamics of neuronal deformation during action potential, PNAS 117 (19) 10278-10285 (2020).

[34] Lyskov, E., Effect of 45 Hz magnetic fields on functional state of the human brain, Bioelectromagnetics, 14(2), 87-95 (1993).

[35] Marcolli, M., Gamma Spaces and Information, J. Geom. Phys, 140, 26-55 (2019).

[36] Mumford, D., Theta characteristics of an algebraic curve, Annales scientifiques de l'École Normale Supérieure, Vol 4, Issue 2, 181-192 (1971).

[37] Mumford, D., Tata Lectures on Theta, Vol 2, Chapter 3, Birkhauser (1987).

[38] Munkres, J., Introduction to Topology, Chapter 12, Prentice Hall International Edition (2014) .

[39] Mussel, M., Schneider, M., It sounds like an action potential: unification

of electrical, chemical and mechanical aspects of acoustic pulses in lipids, Journal of the Royal Society Interface, Vol 16, Issue 151 (2019).

[40] Nash,C.,Sen, S., Topology and Geometry for Physicists, Dover (2011).

[41] Newell,A.,Solitons in Mathematics and Physics,SIAM,1 June(1985)

[42] O'Raifeartaigh, L., The Dawning of Gauge Theory, PUP (1997).

[43] Ortego-de San Luis, R., Ryan, T., Understanding the physical basis of memory: Molecular mechanisms of the engram, Journal pf Biological Chemistry, Vol 298 Issue 5, 101866 (2022).

[44] Petrov, A., Sachs, F., Flexoelectricity and elasticity of asymmetric biomembranes, Physical Review E, 65, 021905 (2002).

[45] Purcell, E., Low Reynold Numbers Physics, Am. J. Phys, 45, 3-11 (1977).

[46] Queenan,B., Ryan, T., Gazzanega, M., Gallistel, C., On the research of time past:The hunt for the substrate of memory, Annals of the New York Academy of Sciences, 1396, 108-125 (2017).

[47] Raina, A.,Sen.S, Grassmanians and the Multiplicative Ward Identity, Phys Lett B, 203, 256 (1988).

[48] Regan, D., Williams, J., Borri, P., Langbein, W., Lipid Bilayer Thickness Measured by Quantitative DIC Reveals Phase Transitions and Effects of Substrate hydrophillicity, Langmuir, 35, 43, 13805-13814 (2019).

[49] Reimann, M.,Nolte.M,Scolamiero,M,Turner.K, Perin.R,Chindemi.G,Dlotko.P,Levi.R,Hess.K,Markram.H,(2017), Cliques of Neurons bound into Cavities Provide a Missing Link between Structure and Function, Frontiers in Computational Neuroscience, Vol 11, Art

48 (2017).

[50] Ryan, T., Ortega de San Luis, C., Pezzoli, M., Sen, S., Engram cell connectivity: an evolving substrate for information storage, Current Opinions in Neurobiology, 67:215-227 (2021)

[51] Barry.,J.,Turner,M.,Scholl,J.,Optical magnetic detection of single action potentials using quantum defects in diamond,PNAS,113(49),14133-14138(2016)

[52] Scott.A, Neuroscience: A Mathematical Primer, Springer-Verlag, New York (2002).

[53] Segal.J., Surface Charge of Giant Axons of Squid and Lobster, Biophys.J, 470-489 (1968).

[54] Sengupta, B., Tozzi, A., Cooray, G., Douglas, P., Friston, K., Towards a Neuronal Gauge Theory, PLOS 14(3), e1002400 (2016).

[55] Shrivastava, S., Schneider, M., Evidence for two-dimensional solitary sound waves in a lipid controlled interface and its implications for biological signalling, The Royal Society Interface, Vol 11, Issue 97 (2014).

[56] Sterratt, D., Goldman-Hodgkin-Katz,Equation, Encyclopedia of Computational Neuroscience, New York (2014).

[57] Tansey, J., Biochemistry Vol 1 p 143, John Wiley and Sons (2019).

[58] Teleman, C., Riemann Surfaces, math.berkeley.edu/ teleman/math/Riemann.pdf (2003).

[59] Tonnegawa, S., Pignatelli, M., Roy, D., Ryan, T., Memory engram storage and retrieval, Current Opinions in Neorobiology, 35, 101-109 (2015).

[60] Tozzi, A., Yurkin, A., Peters, J., A Geometric Milieu Inside the Brain, Foundations of Science, https://doi.org/10.1007/s10699-21-09798-x (2021).

[61] Tsien, R., Very long-term memories may be stored in the pattern of holes in the perineuronal net, PNAS, 110(30) 12456-12461 (2013).

[62] Uchida, M., Onose, Y., Matsui, Y., Tokura, Y., Real Space observation of helical spin order, Science 311, 359 (2006).

[63] Yusupov,J.,Sabirov,K.,Ehrhardt,M.,Matrasulov,D.,arXiv:1903.04250v1[nlin.PS]26Feb